

## Quasideuteron effect with a polarized $\vec{\gamma}$ -ray beam

D. Babusci,<sup>1</sup> V. Bellini,<sup>2,3</sup> M. Capogni,<sup>4,5</sup> L. Casano,<sup>4</sup> B. Currò Dossi,<sup>6</sup> A. D'Angelo,<sup>4</sup> D. A. De Lima,<sup>7</sup> F. Ghio,<sup>8,9</sup> B. Girolami,<sup>8,9</sup> L. Hu,<sup>4</sup> W. Leidemann,<sup>6</sup> F. Lugaresi,<sup>5</sup> D. Moricciani,<sup>4</sup> G. Orlandini,<sup>6,10</sup> P. Picozza,<sup>4,5</sup> and C. Schaerf<sup>4,5</sup>

<sup>1</sup>Istituto Nazionale di Fisica Nucleare—Laboratori Nazionali di Frascati, Via Enrico Fermi 40, I-00044 Rome, Italy

<sup>2</sup>Dipartimento di Fisica dell'Università di Catania, Corso Italia 57, I-95129 Catania, Italy

<sup>3</sup>Istituto Nazionale di Fisica Nucleare—Laboratori Nazionali del Sud, Viale S. Sofia 44, I-95125 Catania, Italy

<sup>4</sup>Istituto Nazionale di Fisica Nucleare—Sezione di Roma2, Via della Ricerca Scientifica 1, I-00133 Rome, Italy

<sup>5</sup>Dipartimento di Fisica dell'Università di Roma "Tor Vergata," Via della Ricerca Scientifica 1, I-00133 Rome, Italy

<sup>6</sup>Dipartimento di Fisica dell'Università di Trento, I-38050 Povo, Trento, Italy

<sup>7</sup>Departamento de Fisica, Universidade Federal de Paraíba, 5800 João Pessoa (PB), Brazil

<sup>8</sup>Istituto Superiore di Sanità, Viale Regina Elena 299, I-00161 Rome, Italy

<sup>9</sup>Istituto Nazionale di Fisica Nucleare—Sezione Sanità, Viale Regina Elena 299, I-00161 Rome, Italy

<sup>10</sup>Istituto Nazionale di Fisica Nucleare—Sezione di Padova, Gruppo Collegato di Trento, I-38050 Povo, Trento, Italy

(Received 16 April 1996)

The  $^{28}\text{Si}(\vec{\gamma},np)X$  reaction has been studied using the Ladon polarized and tagged  $\gamma$ -ray beam, in the energy region between 50 and 75 MeV. The data have been compared with the *quasideuteron* mechanism. At the highest photon energy the applied model leads to a satisfactory description of both the unpolarized cross section and beam polarization asymmetry. [S0556-2813(96)04909-6]

PACS number(s): 25.20.Dc, 21.30.Fe, 24.70.+s, 29.27.Hj

### I. INTRODUCTION

The *quasideuteron* mechanism of photon absorption in complex nuclei in the energy region  $E_\gamma = 40\text{--}80$  MeV has been extensively investigated in the past. In this work we study for the first time the  $(\vec{\gamma},np)$  reaction on an intermediate nucleus with polarized photons. The energy region above the giant dipole resonance is the so-called *quasideuteron* region since it has been interpreted with the idea that an incoming photon is absorbed predominantly by a correlated pair of nucleons of the target nucleus, while the other nucleons act as spectators. The name "quasideuteron" stems from the original work of Levinger [1] in 1951, where he supposed the pair to be constituted by a neutron and a proton. The nuclear photoabsorption cross section was written in terms of the deuteron photodisintegration cross section as follows:

$$\sigma_{\text{qd}}(E_\gamma) = L \frac{NZ}{A} \sigma_D(E_\gamma). \quad (1.1)$$

The fact that in nuclei the  $(\gamma,np)$  process is much more important than  $(\gamma,nn)$  or  $(\gamma,pp)$  reactions is based mainly on two considerations: (i) The dominant electric dipole transition is suppressed for  $n$ - $n$  and  $p$ - $p$  pairs and (ii) the Pauli exclusion principle allows only one  $S$ -wave singlet state for the  $n$ - $n$  or  $p$ - $p$  systems, but four states (one singlet and three triplet) for the  $n$ - $p$  system.

The  $(\gamma,np)$  reaction is, of course, the privileged tool for the determination of the contribution of the *quasideuteron* mechanism. Since the dynamics of the  $n$ - $p$  pairs in nuclei is different from that of the free ones, i.e., the deuterons, this reaction also allows the study of the nucleon-nucleon dynamical correlations in the nuclear ground state.

After Levinger, several versions of the *quasideuteron* model were given in the literature [2–7], which tried to improve the model with respect to various physical aspects (Pauli blocking, Fermi motion of the pair, binding energy, etc.). In recent years the model has been revisited [8–10] and emphasis has been put on the role of meson exchange currents (MEC's) and on the distortion of the wave functions of the photoemitted nucleons due to the final state interaction (FSI).

In this paper we present the experimental data on the  $(\vec{\gamma},np)$  reaction, collected using the Ladon [11,12] polarized and tagged photon beam produced at the Frascati National Laboratory of the Istituto Nazionale di Fisica Nucleare (INFN), an active target of  $^{28}\text{Si}$ , and a series of proton and neutron detectors. The experimental setup and the data analysis procedure are described in Secs. II and III, respectively. The experimental results are presented in Sec. IV and are interpreted in Sec. V, making use of a modified Levinger model.

### II. EXPERIMENTAL SETUP

The experimental data were collected using the Ladon [11,12] polarized and tagged photon beam produced by the backward Compton scattering of laser light against the high energy electrons circulating in the storage ring ADONE at the Frascati National Laboratory of INFN.

#### A. Ladon $\vec{\gamma}$ beam

One of the most interesting features of the Compton back-scattered  $\vec{\gamma}$  ray beam is the polarization. Since for ultrarelativistic electrons helicity is a good quantum number, electrons cannot flip their spin during the Compton scattering. Moreover, for scattering in the backward direction there is

not even transfer of orbital angular momentum from the electrons to the photons. Therefore  $\vec{\gamma}$  rays with energy close to the allowed maximum value (in this experiment corresponding to  $E_{\gamma}^{\max}=78.7$  MeV) retain the same polarization as the initial laser photons.

To measure the energy of the  $\vec{\gamma}$  beam we use an internal tagging system, where the scattered electrons are momentum analyzed by one dipole magnet and one quadrupole of the storage ring lattice. The tagging counter consists of a silicon solid-state microstrip detector composed of 96 vertical strips with a pitch of  $650\mu\text{m}$ , backed by a fast plastic scintillator.

The energy resolution of the  $\vec{\gamma}$  beam depends on the energy of the scattered electrons and on the energy of the electrons circulating in the storage ring. The energy resolution of the Ladon beam is of the order of  $\sigma_{E_{\gamma}}=2$  MeV [12].

The photon flux has been measured using a  $25.4\text{ cm} \times 25.4\text{ cm}$  NaI detector, with 100% efficiency.

### B. Active target and detectors

The nucleus  $^{28}\text{Si}$  was chosen as a target for the following reasons: (1) to study the validity of the quasideuteron model in a medium-heavy nucleus, since it has already been studied in light nuclei as  $^4\text{He}$ ,  $^6\text{Li}$ ,  $^9\text{Be}$ ,  $^{12}\text{C}$ , and  $^{16}\text{O}$  [13–17] and in a heavy nucleus as  $^{208}\text{Pb}$  [18], and (2)  $^{28}\text{Si}$  can be built into a solid-state detector and therefore constitutes an active target which provides a signal proportional to the energy deposited in it.

The target is a cylindrical solid-state detector of 24 mm diameter and 3 mm thickness. To increase the thickness exposed to the beam, the target is rotated by an angle of  $20^\circ$  with respect to the beam direction.

The proton detectors consist of a telescope of three cylindrical silicon solid-state detectors located at an angle of  $53.3^\circ$  with respect to the beam direction and at a distance of 30 mm from the center of the target. The diameter of these three detectors is 24 mm and their thicknesses are 2, 5, and 5 mm, respectively. The energy resolution of these detectors for  $\alpha$  particles is  $\Delta E \approx 60$  keV [full width at half maximum (FWHM)] (this result was obtained using a  $^{241}\text{Am}$  source). The target and the proton detectors are in a vacuum chamber, with a pressure of the order of  $10^{-3}$  bars.

The neutron detectors consist of five organic liquid scintillators (NE213), located at a distance from the target  $D=60$  cm and at angles  $\vartheta_n=22^\circ, 55.5^\circ, 90^\circ, 125^\circ,$  and  $157^\circ$  with respect to the beam direction. Both the proton and the neutron detectors cover a solid angle of 0.13 sr. A time of flight (TOF) resolution  $\Delta T \approx 1.3$  ns (FWHM) between the target and each of the neutron detectors has been measured using a  $^{60}\text{Co}$  source. This value allows the determination of the neutron kinetic energy with sufficient resolution. The timing calibration is obtained by the comparison of the neutron TOF with that of the photons produced by electromagnetic (e.m.) background reactions. Defining  $\tilde{t}=t_{\gamma}-t_n$  the time of flight difference between the neutron and the  $\gamma$ , the kinetic energy of the neutron is given by

$$T_n = M_n \left( \sqrt{1 + \frac{D^2}{c^2 \tilde{t}^2 + 2Dc\tilde{t}}} - 1 \right). \quad (2.1)$$

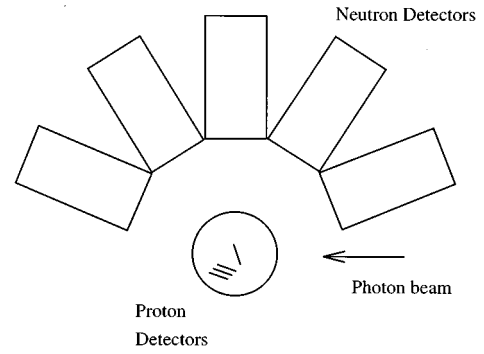


FIG. 1. Sketch of the experimental setup.

The experimental setup is shown in Fig. 1. Using the described apparatus we have measured the energy distribution of the protons emitted in the  $(\vec{\gamma},p)$  reaction, the energy and angular distributions of the neutrons emitted in the  $(\vec{\gamma},n)$  reaction, and the correlated energies and angular distributions as well as the angular correlation  $\vartheta_{n-p}$  for the protons and neutrons emitted in the  $(\vec{\gamma},np)$  reaction.

### III. DATA ANALYSIS

The procedure of the data analysis consists of three steps: (1) calibration of the tagging system, of the active target, and of the proton and of the neutron detectors and determination of their efficiencies; (2) analysis of the  $(\vec{\gamma},p)$  and the  $(\vec{\gamma},n)$  data to determine the maximum energy correctly detected for the proton and the neutron, respectively; and (3) analysis of the  $(\vec{\gamma},np)$  data and determination of the polarized differential cross sections.

The tagging calibration is determined by using a magnetic pair spectrometer in coincidence with the tagging detector. In our energy range the tagging response is represented by a linear relation, as illustrated in [11] and [12].

The determination of the neutron detectors efficiency has been obtained using a Monte Carlo code which takes into account all the nuclear reactions induced by the incoming neutron on the protons and the  $^{12}\text{C}$  nuclei that constitute the detector [19–21]; experimental effects due to the noise and the nonlinearities of the electronics have also been taken into account.

The data analysis of the  $(\vec{\gamma},p)$  and  $(\vec{\gamma},n)$  reactions follows two different steps: (1) rejection of the e.m. background events and (2) identification of the  $(\vec{\gamma},p)$  or  $(\vec{\gamma},n)$  events. To reject the e.m. events we make full use of the detector response. For the neutrons we use the head-tail<sup>1</sup> technique, discussed in [22–25]. This is based on the fact that the form of light pulse due to a hadron has a larger tail than that due to an electron or a photon. Figure 2 shows the separation between the nuclear and the e.m. events. The protons detected in the solid-state silicon detectors telescope are identified by means of the  $\Delta E-E$  technique, where we consider

<sup>1</sup>Head is defined as the total charge of the pulse while the tail is defined as the charge integrated after a delay of 30 ns with respect to the pulse peak.

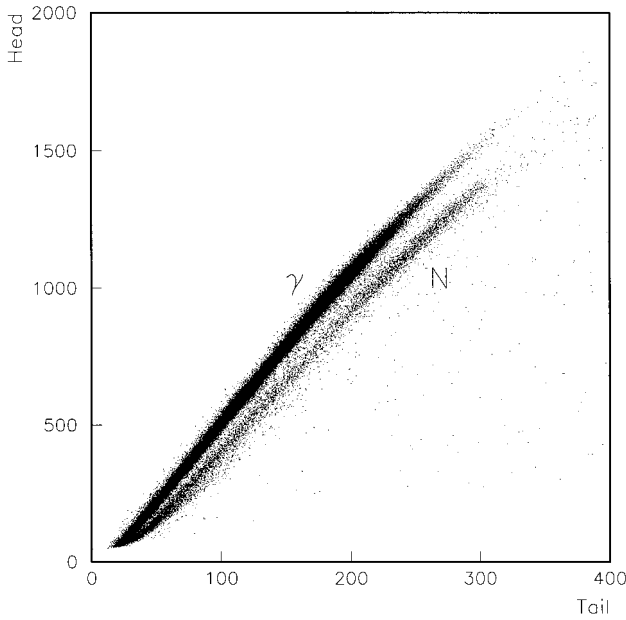


FIG. 2. Typical head-tail plot used for the separation of neutrons and photons. The total charge collected is plotted as a function of the portion of the tail in the pulse.

the correlation between the energy  $\Delta E$  lost by a charged particle in the first silicon detector of the telescope and the total detected energy  $E$  of the same particle obtained as the sum of the energies deposited in the three detectors of the telescope. The events where the protons are detected by the telescope are clearly separated from those due to the detection of deuterons or electrons. The energy spectra related to events where protons and electrons have been identified are shown in Fig. 3. To identify the nuclear events from the reaction channels  $(\vec{\gamma}, p)$  or  $(\vec{\gamma}, n)$ , we use a global event reconstruction procedure, which makes full use of the two-

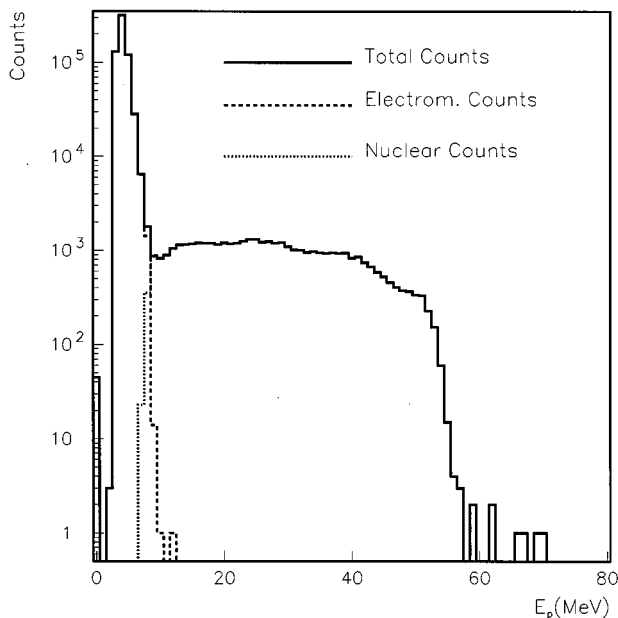


FIG. 3. Proton energy spectra for the  $^{28}\text{Si}(\vec{\gamma}, p)X$  reaction.

body kinematics constraints. Fixing the incoming photon energy  $E_\gamma$  and the outgoing nucleon direction ( $\vartheta_{n/p}$  and  $\varphi_{n/p}$ ) the kinematics of the reaction is completely determined, if the residual nucleus is left in its ground state. Under these hypotheses it is also possible to determine the kinetic energies  $T_{p/n}$  of the outgoing nucleon and  $T_{\text{recoil}}$  of the recoiling nucleus. We may define the following functions:

$$\chi^2(E_\gamma^{\text{theor}}, \vartheta_n^{\text{theor}}) = \frac{(E_\gamma^{\text{expt}} - E_\gamma^{\text{theor}})^2}{\sigma_{E_\gamma}^2} + \frac{(\vartheta_n^{\text{expt}} - \vartheta_n^{\text{theor}})^2}{\sigma_{\vartheta_n}^2} + \frac{(T_n^{\text{expt}} - T_n^{\text{theor}})^2}{\sigma_{T_n}^2} \quad (3.1)$$

for the  $(\vec{\gamma}, n)$  reaction and

$$\chi^2(E_\gamma^{\text{theor}}, \vartheta_p^{\text{theor}}, \varphi_p^{\text{theor}}) = \frac{(E_\gamma^{\text{expt}} - E_\gamma^{\text{theor}})^2}{\sigma_{E_\gamma}^2} + \frac{(\vartheta_p^{\text{expt}} - \vartheta_p^{\text{theor}})^2}{\sigma_{\vartheta_p}^2} + \sum_{i=1}^3 \frac{[T_p^{\text{expt}}(i) - T_p^{\text{theor}}(i)]^2}{\sigma_{T_p}^2(i)} \quad (3.2)$$

for the  $(\vec{\gamma}, p)$  reaction. The quantities with superscript ‘‘expt’’ are those experimentally measured while the quantities with superscript ‘‘theor’’ are calculated using the energy and momentum conservation for the reactions under consideration, as a function of  $E_\gamma^{\text{theor}}$ ,  $\vartheta_{n/p}^{\text{theor}}$ , and  $\varphi_{n/p}$ . The quantities  $\sigma_{E_\gamma, \vartheta_{n/p}, T_{n/p}}$  are the experimental uncertainties. For the  $(\vec{\gamma}, p)$  reaction  $T_p(i)$  are the energies lost by the proton in each of the solid-state detectors of the telescope.

By minimizing the function  $\chi^2$  with respect to  $E_\gamma^{\text{theor}}$ ,  $\vartheta_{n/p}^{\text{theor}}$ , and  $\varphi_{n/p}$  we are able to identify the  $(\vec{\gamma}, p)$  and  $(\vec{\gamma}, n)$  reaction channels by selecting the events with a cut on the minimum value of the  $\chi^2$  function. The reconstructed value of the recoil kinetic energy  $T_{\text{recoil}}$  may be used to obtain the value of the missing energy  $e_m = E_\gamma - T_{n/p} - T_{\text{recoil}}$ , whose distribution for the  $(\vec{\gamma}, p)$  and the  $(\vec{\gamma}, n)$  reactions is shown in Figs. 4 and 5, respectively. This procedure also enables us to determine the maximum values for the neutron and proton energies correctly detected by the experimental apparatus. These values, identified by a constraint on the missing energy, correspond to  $E_p^{\text{max}} \approx 65$  MeV and  $E_n^{\text{max}} \approx 60$  MeV. The events coming from the  $(\vec{\gamma}, np)$  reaction are selected among those where a proton and a neutron are detected in coincidence in two arms of the apparatus. The protons are identified by the  $\Delta E$ - $E$  criteria described above, while the neutrons are selected from the TOF information. The most interesting result that we find is related to the energy distribution of the two nucleons emitted in this reaction. The energy spectrum of the protons is peaked at  $\sim 25$  MeV [corresponding to  $(E_\gamma^{\text{max}} + Q)/2$ ], while that of the neutrons is peaked at  $\sim 5$  MeV, as illustrated in Fig. 6. This unexpected result has been confirmed by another experiment performed by Grabmayr [26] using the tagged photon beams of Mainz (MAMI-A) [27] at  $E_\gamma \sim 140$  MeV and Lund (MAXLAB) [28] at  $E_\gamma \sim 75$  MeV. Figure 7 shows the missing energy  $e_m = E_\gamma - T_p - T_n$  for the  $(\vec{\gamma}, np)$  reaction.

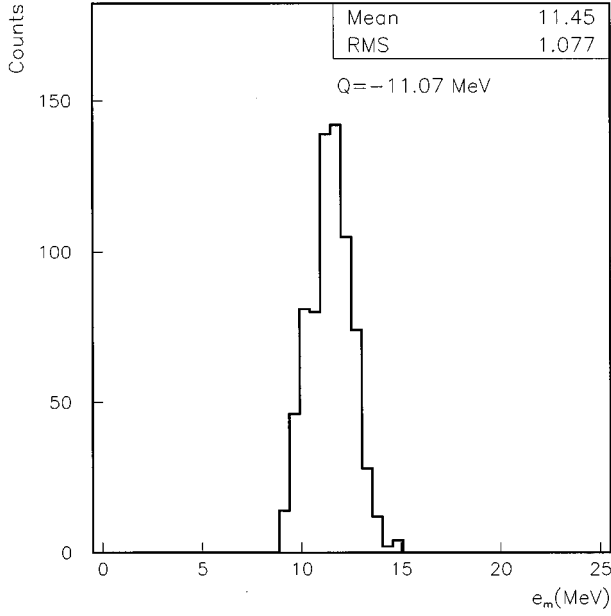


FIG. 4. Distribution of the missing energy for the reaction  $(\vec{\gamma}, p)$ , compared with the c.m. energy threshold  $Q = M_{^{28}\text{Si}} - M_{^{27}\text{Al}} - M_p$ .

#### IV. EXPERIMENTAL RESULTS

The experimental cross section for the  $(\vec{\gamma}, np)$  reaction has been calculated according to the following relation:

$$\frac{d^2\sigma}{d\Omega_p \Omega_n} = \frac{N_{ev}}{N_\gamma \ell \rho \Delta\Omega_p \Delta\Omega_n \varepsilon_n}, \quad (4.1)$$

where  $N_{ev}$  represents the nuclear events selected using the procedure illustrated in the previous section,  $N_\gamma$  is the num-

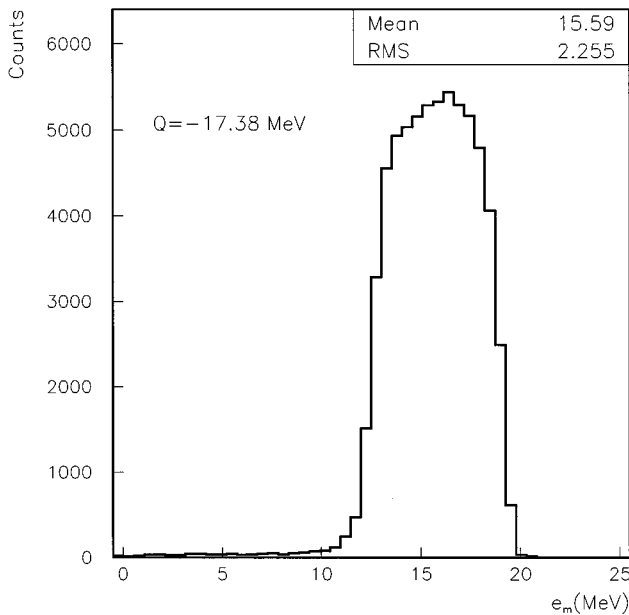


FIG. 5. Distribution of the missing energy for the reaction  $(\vec{\gamma}, n)$ , compared with the c.m. energy threshold  $Q = M_{^{28}\text{Si}} - M_{^{27}\text{Si}} - M_n$ .

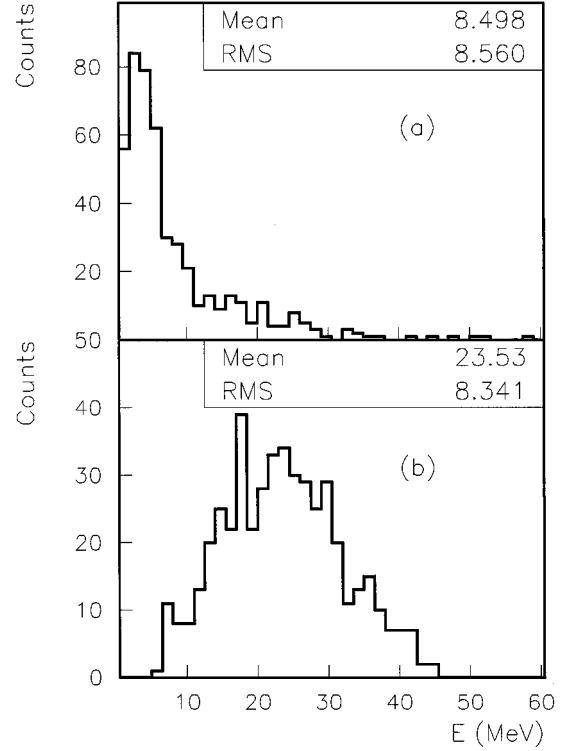


FIG. 6. Energy distribution of the neutrons (a) and the protons (b) for the  $^{28}\text{Si}(\vec{\gamma}, np)X$  reaction.

ber of incoming photons,  $\ell$  and  $\rho$  (expressed in nuclei/cm<sup>3</sup>) are the target length and density,  $\Delta\Omega_p$  and  $\Delta\Omega_n$  are the solid angles covered by the proton and the neutron detectors, respectively, and  $\varepsilon_n$  is the efficiency of the neutron detector. The product  $\Delta\Omega_p \Delta\Omega_n$  is derived from a Monte Carlo simulation which takes into account the finite dimensions of the target, and of the proton and neutron detectors.

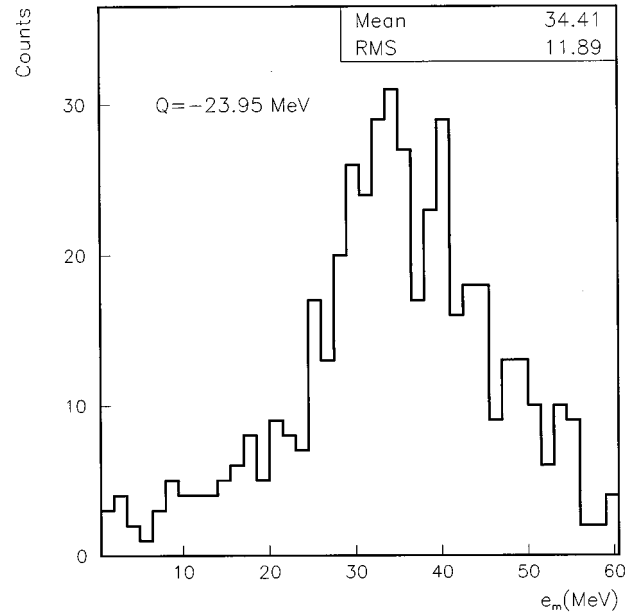


FIG. 7. Distribution of the missing energy for the reaction  $^{28}\text{Si}(\vec{\gamma}, np)X$ , compared with the c.m. energy threshold  $Q = M_{^{28}\text{Si}} - M_{^{26}\text{Al}} - M_n - M_p$ .

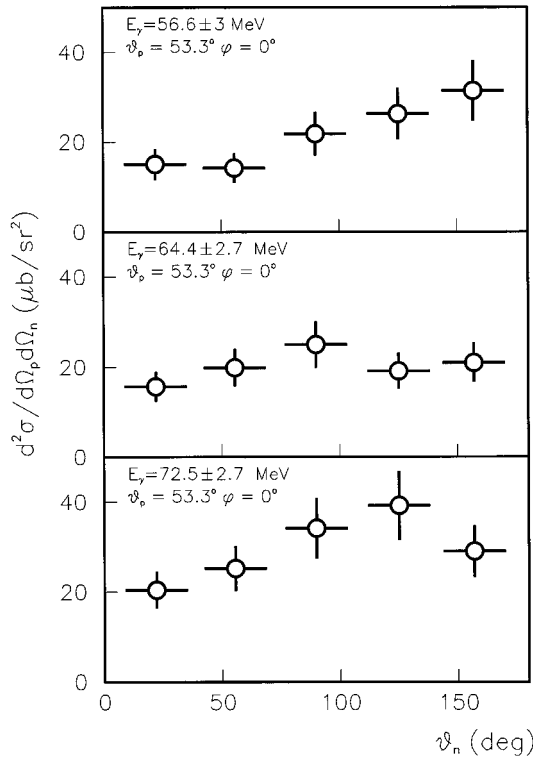


FIG. 8. Differential cross section for the  $^{28}\text{Si}(\vec{\gamma},np)X$  reaction for incoming photons with linear polarization parallel to the plane defined by the outgoing proton and neutron in the laboratory frame ( $\varphi=0^\circ$ ).

Figures 8 and 9 show the experimental results for the differential cross section of the  $(\vec{\gamma},np)$  reaction, for incoming photons with polarization parallel and perpendicular, respectively, with respect to the plane defined by the outgoing protons and neutrons in the laboratory frame. The results are plotted as functions of the angle  $\vartheta_n$ , for three different energy bins. In Figs. 10 and 11 the unpolarized differential cross section and the  $\vec{\gamma}$  asymmetry  $\Sigma = (\sigma_{\parallel} - \sigma_{\perp}) / (\sigma_{\parallel} + \sigma_{\perp})$ , respectively, are represented and compared with our model predictions as described in Sec. V.

## V. RESULTS OF A PHENOMENOLOGICAL MODEL

For the interpretation of the experimental data we start from the usual idea that the photon reacts directly with a quasideuteron pair. However, because of the large missing energy in the experiment ( $e_m \approx 35$  MeV), the reaction cannot be thought of as a clean quasideuteron process. Still one may use this picture and assume that due to the FSI the  $n-p$  pair is losing energy and momentum interacting with the rest nucleus. Here we consider such a FSI in the most simple way. We do not employ any dynamical model, but in calculating the pair cross section we simply take into account losses of energy and momenta by using the experimentally measured values of these quantities for the final  $n-p$  pair. Therefore the pair cross section is not given any more by the deuteron photodisintegration, because there would be no match between photon energy and final  $n-p$  energy. As a matter of fact one ends up with a condition which is more

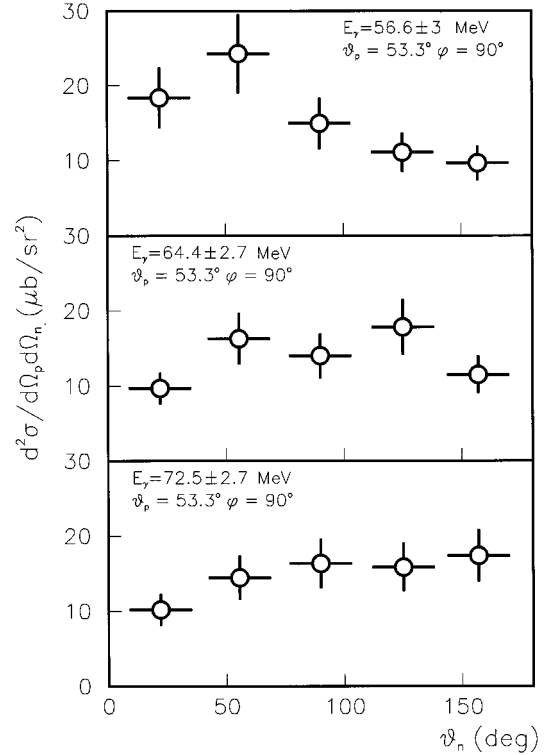


FIG. 9. Differential cross section for the  $^{28}\text{Si}(\vec{\gamma},np)X$  reaction for incoming photons with linear polarization perpendicular to the plane defined by the outgoing proton and neutron in the laboratory frame ( $\varphi=90^\circ$ ).

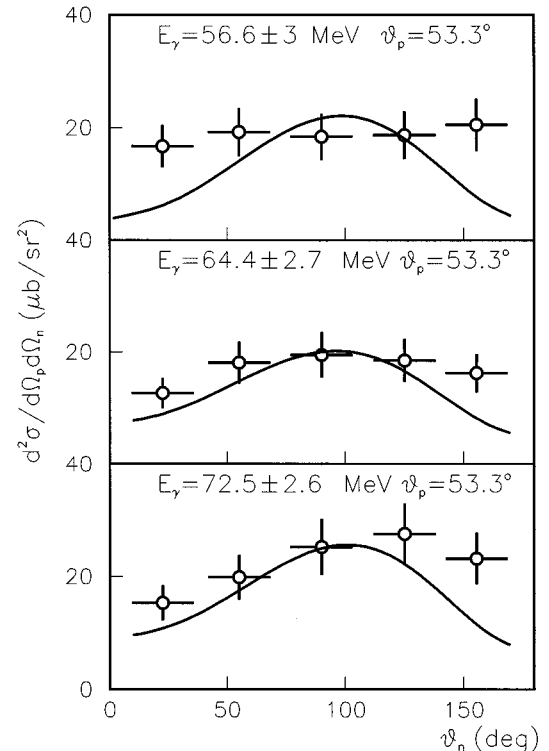


FIG. 10. Model results and experimental data for the unpolarized cross section.

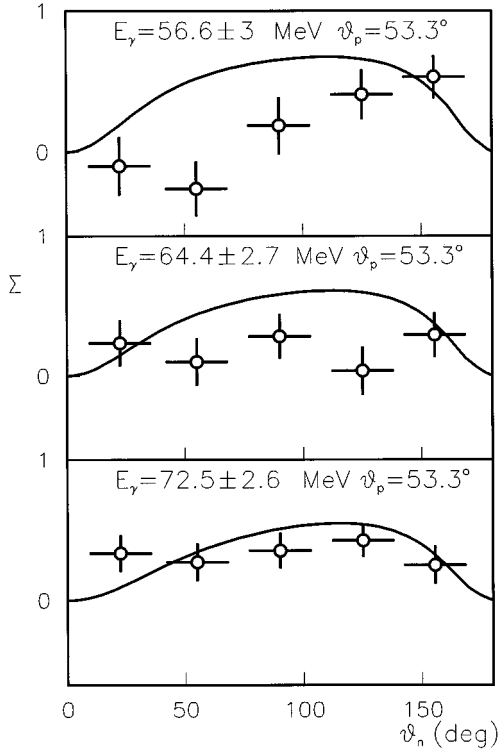


FIG. 11. Model results and experimental data for the  $\vec{\gamma}$  asymmetry.

similar to electron scattering, namely, with less energy than momentum transfer. However, one should bear clearly in mind that also in our model the photon initially transfers equal amounts of energy and momentum. We only assume that the  $n$ - $p$  pair loses energy and momentum due to the FSI with the rest nucleus. In this way we use a final  $n$ - $p$  pair wave function with the correct asymptotic behavior. Considering also the center of mass (c.m.) motion of the  $n$ - $p$  pair one gets the following expression for the nuclear cross section:

$$\begin{aligned} \frac{d\sigma^A}{d\Omega_n}(E_\gamma, \Omega_n) &= L' \frac{NZ}{A} \int d\vec{P} n^{[2]}(\vec{P}) \\ &\times \left[ \frac{d\sigma}{d\Omega_n^{\text{c.m.}}}(E_\gamma^{\text{c.m.}}, E_{np}^{\text{c.m.}}, \Omega_n^{\text{c.m.}}) \right]_{\text{pair}} \\ &\times \left( \frac{d\Omega_n^{\text{c.m.}}}{d\Omega_n}(\vec{P}, \vec{k}, \Omega_n) \right), \end{aligned} \quad (5.1)$$

where  $E_\gamma = ck$  is the photon energy,  $E_{np}^{\text{c.m.}}$  is the relative kinetic energy of neutron and proton in the final pair c.m. system, and  $L'NZ/A$  is the usual factor introduced in quasi-deuteron models. Moreover,  $\vec{P}$  denotes the initial momentum of the c.m. of the pair,  $n^{[2]}$  is the pair c.m. momentum distribution, and  $d\Omega_n^{\text{c.m.}}/d\Omega_n$  is the Jacobian of the transformation from the pair c.m. to the laboratory system. Because of the above-mentioned difference of our model compared to Levinger's model, i.e., no deuteron photodisintegration cross section as input,  $L'$  can be different from the Levinger factor  $L$ . Furthermore, one should note that  $E_{np}^{\text{c.m.}}$  and  $E_\gamma^{\text{c.m.}}$  are

uniquely determined from given  $E_\gamma$ ,  $\vec{P}$ , and neutron, and proton momenta. Because of the large missing mass, one obtains in this way also a rather large difference between  $E_{np}^{\text{c.m.}}$  and  $E_\gamma^{\text{c.m.}}$ .

The pair cross section is calculated taking into account contributions due to nonrelativistic one-body currents, Siegert operator, MEC, isobar configurations, and relativistic corrections (spin-orbit current) [29].

The pair c.m. momentum distribution is defined as

$$\begin{aligned} n^{[2]}(\vec{P}) &= \frac{1}{(2\pi)^6} \int d\vec{r} d\vec{r}' d\vec{R} d\vec{R}' d\vec{p} e^{i\vec{p}\cdot(\vec{r}-\vec{r}')} e^{i\vec{P}\cdot(\vec{R}-\vec{R}')} \\ &\times \rho_{pn}^{[2]}(\vec{r}, \vec{r}'; \vec{R}, \vec{R}'), \end{aligned} \quad (5.2)$$

where  $\vec{r}$  and  $\vec{p}$ ,  $\vec{R}$ , and  $\vec{P}$  are the relative and c.m. positions and momenta of the  $n$ - $p$  pair. The quantity  $n^{[2]}(\vec{P})$  is calculated using the nondiagonal proton-neutron density  $\rho_{pn}^{[2]}(\vec{r}, \vec{r}'; \vec{R}, \vec{R}')$  of the harmonic oscillator model. One obtains

$$\begin{aligned} n^{[2]}(\vec{P}) &= \frac{\pi^{-3/2} \alpha^{-3}}{700\sqrt{2}} \left( \frac{1}{56} \frac{P^8}{\alpha^8} + \frac{3P^6}{7\alpha^6} + \frac{149}{28} \frac{P^4}{\alpha^4} + \frac{205}{7} \frac{P^2}{\alpha^2} \right. \\ &\left. + \frac{6745}{56} \right) e^{-P^2/2\alpha^2}, \end{aligned} \quad (5.3)$$

where  $\alpha = 0.448 \text{ fm}^{-1}$  has been fitted to reproduce the rms radius of  $^{28}\text{Si}$ . The normalization of  $n^{[2]}(\vec{P})$  is

$$\int d\vec{P} n^{[2]}(\vec{P}) = 1. \quad (5.4)$$

In Fig. 10 we show the experimental results for the unpolarized differential cross section compared with the predictions obtained with our model. To have a better comparison to experiment we choose the factor  $L'$  so that the maximum of the theoretical cross section has about the same size as the experimental one. This leads to  $L' = 7$  for the lower two photon energies and to  $L' = 12$  for  $E_\gamma = 72.5 \text{ MeV}$ . The larger  $L'$  at  $E_\gamma = 72.5 \text{ MeV}$  originates from the increasing experimental cross section, while the theoretical cross section decreases from  $E_\gamma = 64.4 \text{ MeV}$  to  $E_\gamma = 72.5 \text{ MeV}$ . Figure 10 illustrates that the phenomenological model cannot reproduce the almost isotropic cross section at  $E_\gamma = 56.6 \text{ MeV}$ . It is readily evident that the comparison becomes better with increasing energy. One finds a rather good agreement at  $E_\gamma = 72.5 \text{ MeV}$ ; only at backward angles is the experimental cross section somewhat underestimated by our model.

The  $\vec{\gamma}$  asymmetry is shown in Fig. 11. Since the asymmetry is given by a ratio of cross sections, it is independent of the factor  $L'$ . Also for the  $\vec{\gamma}$  asymmetry one has a rather large disagreement between experimental results and the model predictions at the lowest energy. At  $E_\gamma = 64.4 \text{ MeV}$  the comparison becomes better, but one still has quite significant differences. However, as for the unpolarized differential cross section one also finds for  $E_\gamma = 72.5 \text{ MeV}$  a rather satisfying agreement between the experimental data and the model results. In conclusion we can say that the additional

photon polarization in the  $(\vec{\gamma}, np)$  reaction leads to further constraints in the quasideuteron interpretation. The fact that two independent observables are described fairly well at the highest photon energy is a strong indication that the quasideuteron reaction is really the dominant mechanism at that energy. The partial failure at lower energies could be due to the greater importance of the FSI. To have a better understanding of the reaction it would be of great interest to have more experimental data at higher energies and for various nuclei. Besides obtaining a further test of the quasideuteron mechanism itself, a more systematic investigation might also

allow one to study the effect of the nuclear  $n$ - $p$  correlation by a proper modification of the  $n$ - $p$  pair wave function.

#### ACKNOWLEDGMENTS

We would like to thank P. Grabmayr for the confirmation of the relatively low neutron energy in  $(\gamma, np)$  reactions. We also would like to thank the technical staff of the Ladon facility (E. Cima, M. Iannarelli, G. Nobili, and E. Turri) for their essential contribution in obtaining a high-quality photon beam.

- 
- [1] J.S. Levinger, Phys. Rev. **84**, 43 (1951).  
 [2] R.R. Wilson, Phys. Rev. **86**, 152 (1952).  
 [3] R.R. Wilson, Phys. Rev. **104**, 218 (1956).  
 [4] K. Gottfried, Nucl. Phys. **5**, 557 (1957).  
 [5] J.S. Levinger, Phys. Lett. **82B**, 181 (1979).  
 [6] J.M. Laget, Nucl. Phys. **A358**, 275c (1981).  
 [7] P. Carlos *et al.*, Nucl. Phys. **A378**, 317 (1982).  
 [8] L. Boato and M.M. Giannini, J. Phys. G **15**, 1605 (1989).  
 [9] S. Boffi and M.M. Giannini, Nucl. Phys. **A553**, 441 (1991).  
 [10] W. Leidemann and G. Orlandini, Nucl. Phys. **A506**, 447 (1990).  
 [11] D. Babusci, E. Cima, M. Iannarelli, E. Turri, F. Basti, I. Halpern, L. Casano, A. D'angelo, D. Moricciani, P.G. Picozza, C. Schaerf, and B. Girolami, Nucl. Instrum. Methods A **305**, 19 (1991).  
 [12] D. Babusci, M. Capogni, L. Casano, A. D'Angelo, F. Ghio, B. Girolami, L. Hu, D. Moricciani, and C. Schaerf, Laboratori Nazionali di Frascati Report No. LNF-95/058(P), 1995, Riv. Nuovo Cimento (to be published).  
 [13] M.W. Wade, M.K. Brussel, L.J. Koester, Jr., and J.H. Smith, Phys. Rev. Lett. **53**, 2540 (1984).  
 [14] S. Homma, Nucl. Phys. **A446**, 241c (1985).  
 [15] I.V. Dogyust, P.I. Vatsset, V.V. Kirichenko, and A.F. Khodyachikh, Sov. J. Nucl. Phys. **35**, 471 (1982).  
 [16] S.N. Dancer, I.J.D. MacGregor, J.R.M. Annand, I. Anthony, G.I. Crawford, S.J. Hall, J.D. Kellie, J.C. McGeorge, R.O. Owens, P.A. Wallace, D. Brandford, S.V. Springham, A.C. Shotter, B. Schoch, J.M. Vogt, R. Beck, and G. Liesenfeld, Phys. Rev. Lett. **61**, 1170 (1988).  
 [17] P.A. Wallace, J.R.M. Annand, I. Anthony, G.I. Crawford, S.N. Dancer, S.M. Doran, S.J. Hall, J.D. Kelly, J.C. McGeorge, I.J.D. Mac Gregor, G.J. Miller, R.O. Owens, J. Vogt, B. Schoch, and D. Branford, Nucl. Phys. **A532**, 617 (1991).  
 [18] R. Bergere, in *Nuclear Physics with Electromagnetic Interactions*, Proceedings, Mainz 1979, Lecture Notes in Physics, edited by H. Arenhövel and D. Drechsel (Springer-Verlag, Berlin, 1979), Vol. 108, p. 138.  
 [19] W.N. Hess, Rev. Mod. Phys. **30**, 368 (1958).  
 [20] V. McLane, C.L. Dunford, and P.F. Rose, *Neutron Cross Section* (Academic Press, New York, 1988), Vol. 2.  
 [21] A. Dal Guerra, Nucl. Instrum. Methods **135**, 337 (1976).  
 [22] P.G. Sjölin, Nucl. Instrum. Methods **37**, 45 (1965).  
 [23] R. Owen, IRE Trans. Nucl. Sci. **5**, 198 (1958).  
 [24] F. Kuchnir and J. Lynch, IEEE Trans. Nucl. Sci. **NS-3**, 107 (1968).  
 [25] F.D. Brooks, Nucl. Instrum. Methods **4**, 151 (1959).  
 [26] P. Grabmayr, in *Proceedings of the 8th Seminar—Electromagnetic Interactions of Nuclei at Low and Medium Energies*, Moscow, 1991, edited by Gurevich Grigory (Institute for Nuclear Research, Moscow, 1992), p. 121.  
 [27] J.D. Kellie, I. Anthony, S.J. Hall, I.J.D. MacGregor, A. MacPherson, P.J. Thorley, S.L. Wan, and F. Zettl, Nucl. Instrum. Methods A **241**, 153 (1985).  
 [28] J.O. Adler, B.E. Andersson, K.I. Blomqvist, B. Forkman, K. Hansen, L. Isaksson, K. Lindgren, D. Nilsson, A. Sandell, B. Schröder, and K. Ziakas, Nucl. Instrum. Methods A **294**, 15 (1990).  
 [29] P. Wilhelm, W. Leidemann, and H. Arenhövel, Few Body Syst. **3**, 111 (1988).